Experimental study of bump effects on boundary-layer transition in compressible high Reynolds number flow

M Costantini[1*], S Risius[1], S Koch[1], C Fuchs[1], U Gerhard[1], S Hein[1] and C Klein[1]

[1] DLR, Institute of Aerodynamics and Flow Technology, Göttingen, Germany

*Marco.Costantini@dlr.de

Abstract

The influence of surface bumps on boundary-layer transition was experimentally investigated in the present work. The experiments were conducted in a (quasi-) two-dimensional flow at low to high subsonic Mach numbers and large chord Reynolds numbers in the low-turbulence Cryogenic Ludwieg-Tube Göttingen. Various streamwise pressure gradients relevant for natural laminar flow surfaces were implemented. Quasi-two-dimensional bumps, with a sinusoidal shape in the streamwise direction (positive half of a sine), fixed length and three different heights, were installed on a two-dimensional flat-plate model. The model was equipped with temperature-sensitive paint for non-intrusive transition detection and with pressure taps for the measurement of the surface pressure distributions. Boundary-layer transition was shown to occur at a more upstream location with increasing bump height-to-length ratio. This was mainly due to the local adverse pressure gradient on the downstream side of the bump, which was particularly pronounced in the case of the bump with the largest height-to-length ratio, thereby inducing boundary-layer separation. In the case of the bump with the smallest height-to-length ratio, bump-induced transition was found to occur at a more downstream location with stronger global flow acceleration; in contrast, the global pressure gradient had no appreciable influence on transition induced by the bump with the largest height-to-length ratio. The effect of the global pressure gradient on transition induced by the medium-sized bump was found to depend on the Mach number.

1 Introduction

Natural Laminar Flow (NLF) technology has been demonstrated to be a powerful tool for drag reduction on aircraft surfaces with zero to moderate sweep angles, where the amplification of streamwise instabilities is the predominant mechanism leading to transition – see Holmes and Obara (1983), Wagner et al. (1989) and Arnal (1992). The drag reduction capability of NLF technology has been verified for a wide range of aircraft classes, from sailplanes to business jets and transport aircraft, as reported in, e.g., Holmes and Obara (1983), Wagner et al. (1989) and Hansen (2010). One of the major concerns about the practicability of NLF technology for aircraft drag reduction is related to the achievability of surface smoothness compatible with NLF requirements. Surface imperfections such as steps, gaps, bumps, waviness, incorrectly installed flush rivets, etc., can affect aircraft surfaces, as discussed in Nayfeh et al. (1988) and Hansen (2010). Already in Holmes and Obara (1983) it had been shown that modern manufacturing techniques for metallic and composite materials can now provide surface smoothness suitable for laminar flow; however, manufacturing tolerances must be specified for the shape and dimension of surface imperfections so that laminar flow can still be achieved. As emphasized in Nayfeh et al. (1988) and Hansen (2010), a guide is needed for size and shape of surface imperfections in order to specify manufacturing tolerances as precisely as possible, thus avoiding overly stringent requirements.

The present work focuses on surface bumps. They can occur, as reported by Wagner et al. (1989) and Hansen (2010), at or between structural joints, ribs, and stringers and in the region of flush rivets. In fact, significant waviness may be found on modern aircraft surfaces only in the form of (widely) spaced bumps.

Criteria for allowable tolerances can thus be developed for this type of imperfection and then extended for multiple bumps. The influence of bumps on boundary-layer stability and transition has been investigated for specific surface geometries and flow conditions in earlier numerical and experimental work, such as in Fage (1943), Nayfeh et al. (1988), Cebeci and Egan (1989), Masad and Iyer (1993) and Perraud (2004), but criteria covering a wide range of boundary-layer stability situations are still not available. In particular, the effect of a variation in the streamwise pressure gradient on bump-induced transition has not been examined up to now. Various stability situations, implemented via a variation of the streamwise pressure gradient, were experimentally investigated in the present work to study the influence of surface bumps on boundary-layer transition in a compressible flow at high Reynolds numbers.

2 Test Conditions and Experimental Setup

The experiments were conducted in a (quasi-) two-dimensional flow at freestream Mach numbers from $M = 0.35$ to 0.77 and chord Reynolds numbers from $Re = 3.5 \cdot 10^6$ to $10 \cdot 10^6$ in the low-turbulence (momentum turbulence level $Tu_{\rho u} \sim 0.06$ %) Cryogenic Ludwieg-Tube Göttingen (DNW-KRG). (For a description of the DNW-KRG wind tunnel and for details on the measurements of the turbulence level in the DNW-KRG test section, see Koch (2004).) Various streamwise pressure gradients relevant for NLF surfaces were implemented in the present work. The Hartree parameter β_H of the self-similar solution of the boundary-layer equations (Falkner-Skan equation) was selected as the characteristic parameter for the global pressure distribution, as suggested, e.g., in Meyer and Kleiser (1989). The investigated range of Hartree parameters was from $\beta_H = -0.012$ (slightly decelerated boundary layer) to 0.102 (accelerated boundary layer). It should be noted here that, by virtue of the working principle of the DNW-KRG Ludwieg-tube facility (see Koch (2004) and Costantini et al. (2016)), the ratio between surface and adiabatic-wall temperatures T_w/T_{aw} was larger than 1 during the test runs: it was in the range $T_w/T_{aw} = 1.040$-1.065 at $M = 0.77$ and decreased to $T_w/T_{aw} = 1.020$-1.040 at $M = 0.35$.

The two-dimensional wind-tunnel model used in the experiments is shown in Figure 1. An available flat-plate configuration, presented in Costantini et al. (2016), was modified to accept exchangeable inserts on the model upper side. The surface bumps were manufactured on the inserts and had a sinusoidal shape (positive half of a sine) in the streamwise direction x. The streamwise extent of the bumps was $a = 20$ mm, i.e., 10 % of the model chord $c = 200$ mm. The start and end of the bumps in the streamwise direction were located at $x/c = 40$ % and 50 %, respectively, with the bump crest being located at $x/c = 45$ %. The bumps were quasi-two-dimensional: their spanwise extent was ten times larger than their streamwise extent, as sketched in Figure 1 (right). The present experimental setup enabled an independent variation of Mach number, Reynolds number, streamwise pressure gradient and bump height, and thus allowed to decouple the effects of changes in the aforementioned parameters on boundary-layer transition.
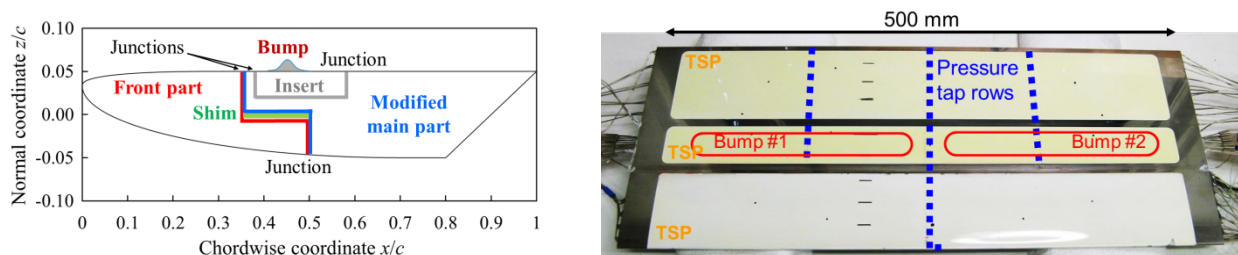

Figure 1: Simplified drawing of the wind-tunnel model construction – side view (left); top view and instrumentation of the wind-tunnel model with leading edge on bottom of the image (right).

Three bumps with different height $h = 0.10$ mm (small bump), 0.24 mm (mid bump) and 0.40 mm (big bump) were examined. They were manufactured on two different inserts: the mid bump was manufactured on the port half of the first insert, which starboard half was left clean (i.e., bump-free) to serve as a reference surface; the small and big bumps were manufactured on the port and starboard halves of the second insert, respectively. As shown in Figure 1 (right), the model was equipped with temperature-

sensitive paint (TSP), a global measurement technique discussed, e.g., in Tropea et al. (2007), and used in the present study for non-intrusive transition detection on the model upper side. TSP formulation, optical setup, leading edge surface quality, acquisition and elaboration of the TSP images were the same as those discussed in Costantini et al. (2016). The model was also instrumented with three rows of pressure taps for the measurement of the surface pressure distributions. Note that the bump regions were equipped with both TSP and pressure taps, thus providing temperature and pressure distributions over the bumps. The mid-span pressure tap row provided a reference pressure distribution in a bump-free area.

3 Results and Discussion

The effect of a larger bump height-to-length ratio on boundary-layer transition is shown in Figure 2 with the TSP results for a case at M = 0.77, Re = 6 · 10^6 and a favorable global pressure gradient (β_H = 0.096). Bright and dark areas (i.e., areas with high and low normalized intensity, respectively) correspond to areas of low and high wall heat flux (and also of low and high wall shear stress), respectively; the detected locations of transition from laminar to turbulent boundary-layer state are indicated in the TSP results by yellow dashed lines. The whitened areas correspond to areas where no TSP had been applied, where the TSP signal-to-noise ratio was too low and/or where the image distortion was too large for sufficiently accurate mapping – see Costantini et al. (2016). Up to four turbulent wedges were caused by the pressure tap rows; the other turbulent wedges arose from contamination of the model surface during wind tunnel operation. In spite of them, natural transition was clearly shown to occur at a more upstream location x_T/c with increasing bump height-to-length ratio h/a – see Figure 2. This result is in agreement with findings from previous experimental (Fage (1943), Perraud (2004)) and numerical work (Nayfeh et al. (1988), Cebeci and Egan (1989), Masad and Iyer (1993), Perraud (2004)).
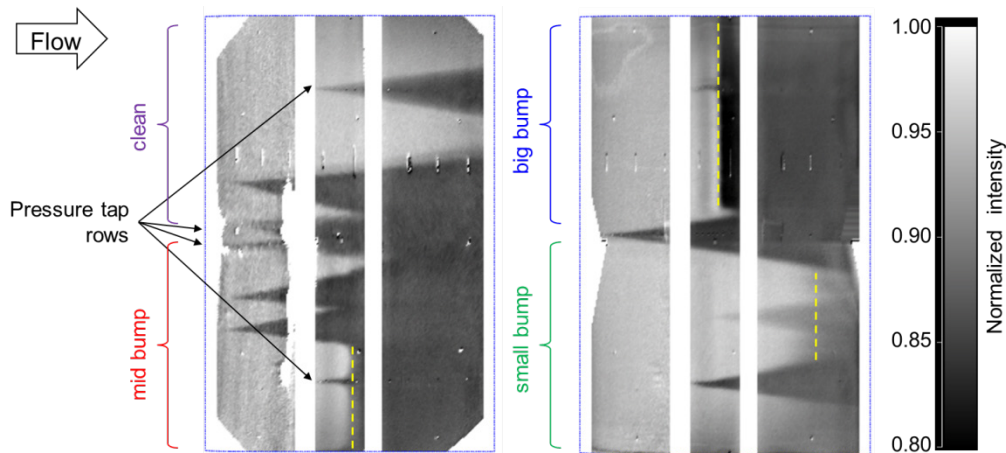

Figure 2: TSP results for different bump height-to-length ratios h/a obtained at M = 0.77, Re = 6 · 10^6 and β_H = 0.096. Clean configuration (bump-free): no transition; small bump (h/a = 0.005): x_T/c = 81 %; mid bump (h/a = 0.012): x_T/c = 51 %; big bump (h/a = 0.020): x_T/c = 49 %. (The difference in the TSP signal-to-noise ratio of the two results is due to different TSP measurement setups used in the experiments).

The surface pressure distributions measured with the two model configurations at the test conditions of Figure 2 are presented in Figure 3. All six pressure distributions (three pressure tap rows for each of the two model configurations) are in excellent agreement for most of the chord length, except for the region around the bumps. (The curves named "Reference (1)" and "Reference (2)" show the pressure distributions measured by means of the mid-span pressure tap row with the model configurations of Figure 2 (left) and Figure 2 (right), respectively.) A zoomed-in plot of the bump region is shown in Figure 3 (right). The presence of the bumps led to significant differences in the pressure distributions, as compared to those obtained with the reference / clean surfaces; the magnitude of these differences clearly increased with increasing bump height-to-length ratio h/a. With respect to its development on the

reference / clean surfaces, the boundary layer was first slightly decelerated when it approached the bumps, then accelerated on the upstream side of the bumps and decelerated on their downstream sides, until the global pressure distribution was finally recovered at a certain distance downstream of the bump end. The exact location of the recovery of the reference / clean surface pressure distribution appears to be more downstream with increasing bump height-to-length ratio. Note that the influence of the local flow acceleration / deceleration over the bumps can be seen also in the TSP results of Figure 2. In fact, the (still laminar) accelerating boundary layer over the upstream side of the bumps was characterized by a higher wall shear stress, and therefore higher wall heat flux, than that of the boundary layer immediately upstream of the start of the bump, resulting in a darker strip in the TSP data at x/c = 40-45 %. Similar, but opposite, considerations apply for the decelerating boundary layer over the downstream side of the bumps, where the wall shear stress (and wall heat flux) lower than that in the surrounding regions led to a brighter strip in the TSP data at x/c = 45-48 % (i.e., immediately downstream of the bump crest). It can be seen in Figure 3 (right) that the deceleration on the downstream side of the bumps was more pronounced than the acceleration on their upstream side; this is in agreement with findings from previous work (see Nayfeh et al. (1988) and Arnal (1992), among others) and eventually induced earlier transition (see Figure 2). As discussed, e.g., in Arnal (1992), Nayfeh et al. (1988), Cebeci and Egan (1989) and Masad and Iyer (1993), the adverse influence of surface bumps on boundary-layer stability and transition is particularly marked when the deceleration on the downstream side of the bump is so strong as to induce flow separation, since amplification of streamwise instabilities is enhanced in separated flow regions. This is the case of the big bump in Figure 2, which was verified via oil film visualizations (not shown here) to lead to a flow deceleration so strong as to induce boundary-layer separation and eventually transition at x_T/c = 49 %, even upstream of the end of the bump. Note that, as a further agreement with previous work, the height-to-length ratio h/a = 0.020 of the big bump is above the critical value of h/a for separation over the downstream side of the bump reported in Nayfeh et al. (1988), Cebeci and Egan (1989) and Masad and Iyer (1993).
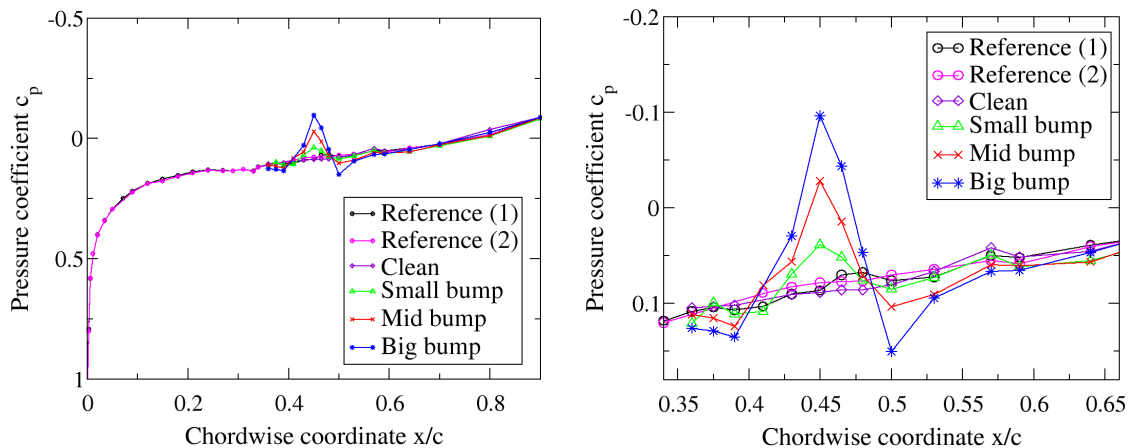

Figure 3: Surface pressure distributions measured for the case of Figure 2. Left: over the whole chord length. Right: zoomed-in around the bump region. Start and end of the bumps are located at x/c = 40 % and 50 %, respectively.

The effect of larger bump height-to-length ratios on boundary-layer transition at all other test conditions examined in the present work was found to be similar to that discussed above.

The influence of a variation in the global pressure gradient on bump-induced transition is shown in Figure 4 with the TSP results for the small and big bumps at M = 0.77 and Re = 6 · 10^6. Three different global pressure gradients were investigated: β_H = 0.063, 0.076 and 0.096. The corresponding TSP results are presented from left to right in Figure 4. As can be seen in this figure, an increase in the Hartree parameter (i.e., a more pronounced global flow acceleration) led to a significant movement of boundary-layer transition into a more downstream location even in the presence of a bump with a height-to-length

ratio of $h/a = 0.005$ (small bump): from $x_T/c = 62\%$ at $\beta_H = 0.063$ to $x_T/c = 81\%$ at $\beta_H = 0.096$. In contrast, a variation of the global pressure gradient was found to have no appreciable influence on boundary-layer transition in the presence of the big bump ($h/a = 0.020$); this was very likely due to the occurrence of transition over a laminar separation bubble induced by the marked adverse pressure on the downstream side of the big bump, which was not affected significantly by a change in the global pressure gradient. In the case of the mid bump (not shown here), the effect of a variation in the global flow acceleration on bump-induced transition was observed to be dependent on the Mach number. At $M = 0.77$, bump-induced transition was essentially unaffected by a change in the global pressure gradient; at lower Mach numbers ($M = 0.35$ and 0.50), stronger flow acceleration led transition in the presence of the mid bump to occur at a more downstream location.
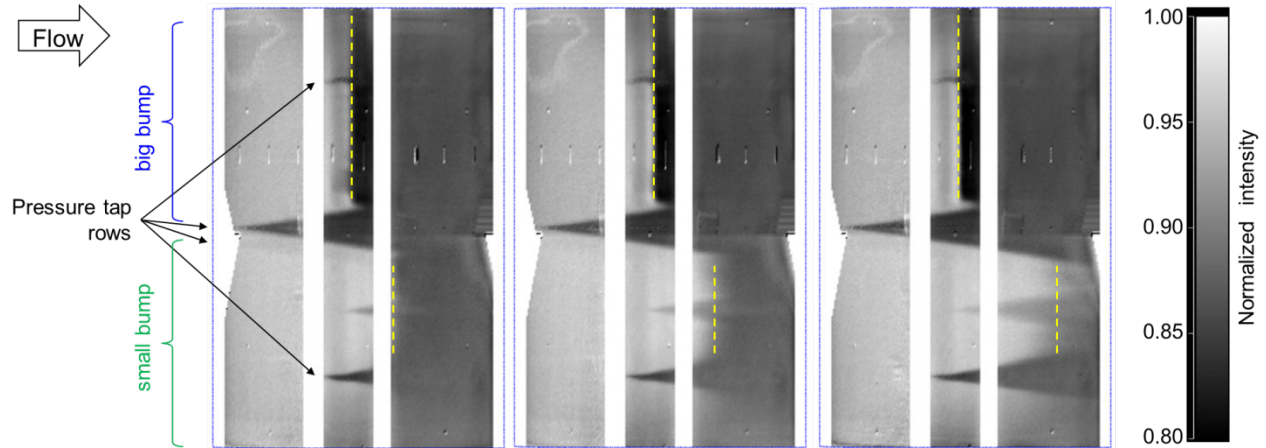

Figure 4: TSP results for different global pressure gradients β_H obtained with the small ($h/a = 0.005$) and big ($h/a = 0.020$) bumps at $M = 0.77$ and $Re = 6 \cdot 10^6$. Left: $\beta_H = 0.063$ ($x_T/c = 62\%$ vs. $x_T/c = 48\%$); center: $\beta_H = 0.076$ ($x_T/c = 68\%$ vs. $x_T/c = 48\%$); right: $\beta_H = 0.096$ ($x_T/c = 81\%$ vs. $x_T/c = 49\%$).

4 Conclusion

The effect of surface bumps on boundary-layer transition was investigated in the low-turbulence Cryogenic Ludwieg-Tube Göttingen by means of the temperature-sensitive paint measurement technique. The experiments were conducted in a compressible (quasi-) two-dimensional flow at subsonic freestream Mach numbers from $M = 0.35$ to 0.77 and chord Reynolds numbers from $Re = 3.5 \cdot 10^6$ to $10 \cdot 10^6$ with various streamwise pressure gradients, relevant for natural laminar flow surfaces. A two-dimensional flat-plate model was modified to accept exchangeable inserts on the model upper side. Quasi-two-dimensional surface bumps, with a sinusoidal shape in the streamwise direction (positive half of a sine), were manufactured on the inserts. The model was also equipped with pressure taps for the measurement of the surface pressure distributions. Three bumps with different height-to-length ratio were examined in this work. The effect of a larger bump height-to-length ratio was to induce boundary-layer transition to occur at a more upstream location; this effect was particularly pronounced in the case of flow separation caused by the local adverse pressure gradient on the downstream side of the bump, with transition occurring even upstream of the end of the bump. The influence of the global streamwise pressure gradient on bump-induced transition was found to be dependent on the bump height-to-length ratio and on the freestream Mach number. In the case of the bump with the smallest height-to-length ratio, stronger global flow acceleration led bump-induced transition to occur at a more downstream location; in contrast, transition induced by the bump with the largest height-to-length ratio was essentially unaffected by the global pressure gradient. The effect of the global flow acceleration on transition induced by the medium-sized bump was dependent on the Mach number. The present results show that the influence of the global streamwise pressure gradient (i.e., of the boundary-layer stability situation) on transition has to be accounted for in criteria for allowable size of bumps on natural laminar flow surfaces.

Acknowledgements

References

Arnal D (1992) Boundary Layer Transition: Prediction, Application to Drag Reduction. *AGARD* R-786: 5-1 to 5-59.

Cebeci T, Egan DA (1989). Prediction of Transition Due to Isolated Roughness. *AIAA Journal* 27(7): 870-875.

Costantini M, Hein S, Henne U, Klein C, Koch S, Schojda L, Ondrus V, Schröder W (2016) Pressure Gradient and Non-adiabatic Surface Effects on Boundary-Layer Transition. *AIAA Journal* 54(11): 3465-3480.

Fage A (1943) The Smallest Size of a Spanwise Surface Corrugation which Affects Boundary-Layer Transition on an Aerofoil. *ARC Reports and Memoranda* 2120.

Hansen H (2010) Laminar Flow Technology – The Airbus View. *Proc. 27th ICAS*: 453-461.

Holmes BJ, Obara, CJ (1983) Observations and Implications of Natural Laminar Flow on Practical Airplane Surfaces. *Journal of Aircraft* 20(12): 993-1006.

Koch S (2004) Zeitliche und räumliche Turbulenzentwicklung in einem Rohrwindkanal und deren Einfluss auf die Transition an Profilmodellen. *DLR FB* 2004-19.

Masad JA, Iyer V (1993) Transition Prediction and Control in Subsonic Flow Over a Hump. *NASA CR* 4543.

Meyer F, Kleiser L (1989) Numerical Investigation of Transition in 3D Boundary Layers. *AGARD* CP-438: 16-1 to 16-17.

Nayfeh AH, Ragab SA, Al-Maaitah AA (1988) Effect of Bulges on the Stability of Boundary Layers. *Physics of Fluids* 31(4): 796-806.

Perraud J (2004) Laminar-turbulent Transition on Aerodynamic Surfaces with Imperfections. *RTO-AVT-111*.

Tropea C, Yarin AL, Foss JF (2007) Springer Handbook of Experimental Fluid Mechanics. Springer-Verlag, Berlin Heidelberg. Chap. 7.4: Transition-Detection by Temperature-Sensitive Paint

Wagner RD, Bartlett DW, Collier Jr. FS (1989) Laminar Flow – The Past, Present, and Prospects. *AIAA Paper* 1989-0989.